BEHAVIOR AND ANALYSIS OF PLATTFORMS BUILDING SYSTEM

by

Bret Albert Burkhart

A thesis submitted to the faculty of
The University of Utah
in partial fulfillment of the requirements for the degree of

Master of Science

Department of Civil and Environmental Engineering

University of Utah

December 2011

STATEMENT OF THESIS APPROVAL

The thesis of **Bret Albert Burkhart**

has been approved by the following supervisory committee members:

Chris Pantelides	, Chair	**12/15/2010**
		Date Approved
Lawrence Reaveley	, Member	**12/15/2010**
		Date Approved
Paul Tikalsky	, Member	**12/15/2010**
		Date Approved

and by **Paul Tikalsky** , Chair of

the Department of **Civil and Environmental Engineering**

ABSTRACT

A new structural building system (Plattforms) was investigated at the University of Utah. The system was analyzed to determine capacity, behavior, and residual strength. Three short span specimens of the system were tested to failure. This thesis addresses the layout of the test specimens as well as their performance under gravity type loading up to ultimate conditions. The thesis also presents a strut and tie method of analysis that may be useful in the development and design of current and new versions of the plattforms building system. The building system offers a prefabricated product to compete with the conventional concrete deck over steel beam floor systems available for construction and design.

TABLE OF CONTENTS

LIST OF FIGURES

LIST OF TABLES

Table Page

ACKNOWLEDGMENTS

First and foremost, I would like to thank my advisor, Dr. Chris P. Pantelides. His expertise, guidance, and encouragement have been instrumental in the completion of this thesis along with the research work involved therein. I would also like to thank my faculty committee members Dr. Lawrence D. Reaveley and Dr. Paul Tikalsky for their further guidance and support.

I also thank my wife, Angela, for her continued support and patience throughout my academic career.

Funding for this project was provided by Plattforms Inc., of Salt Lake City Utah. The design of the test specimens were also provided by Plattforms. Special Thanks To: David Platt, the inventor of the Plattforms system. Darrell Hodgson, head of manufacturing; as well as, Clayton Burningham, and Mark Bryant for their help in the testing lab at the University of Utah.

CHAPTER 1

INTRODUCTION

The Plattforms Building System was tested at the Structures Laboratory of the University of Utah for evaluation of its performance in January 2010. The system is comparable to the three variants of the traditional floor beam system, which have been developed over the years to meet height limitations and the need for complex mechanical installations: composite beams with web openings in the steel beam, composite joists and trusses and stub girders (Viest, 2.5-2.20). The present system consists of a concrete T-section with mechanical blockouts connected to a steel beam at the bottom, where the concrete T-section is connected to a steel beam by nelson studs and welded reinforcing bars.

The typical test specimens were short span versions of the system with lengths of 13 ft-0 in., widths of 4 ft-0 in., and total heights, including the steel beam, of 2 ft-8 in. Mechanical blockouts for the test specimens measured 2 ft-4 in. in width and 1 ft-3 3/8in. in height. A clear image of the layout can be seen in Figure 3.1. Three of these specimens were tested for this evaluation under four-point loading. All of the specimens can be classified as short shear spans with a/d ratios of 2.0 for the first specimen and 1.8 for both the second and third specimens. For code comparison the total load applied to the specimens was related to the effect of a distributed load on the system. This was done by

simply dividing the total load by the area of the deck, and comparing it to ASCE 7 expected live loads for different applications. The worst case loading outlined in ASCE 7 consists of a distributed live load of 250 psf for heavy manufacturing or heavy storage warehouse applications. Using the equivalent effect of a distributed live load of 250 psf over the entire surface of the system, and a load factor of 1.6, the following is concluded: (1) the maximum live load condition falls well within the elastic portion of behavior of the system. At the point of nonlinearity on the load versus displacement curve, the system achieved a capacity of 4.3, 4.9, and 5.1 times the factored surface load, where the variability comes from the two different loading conditions; (2) the displacement at the maximum live load condition was compared to the maximum permissible deflections in ACI 318 for the three specimens. It was found to reach only 15% of the allowable for floors supporting nonstructural elements not likely to be damaged by large deflections to 30% of the allowable for floors supporting nonstructural elements likely to be damaged by large deflections. The system proved to be very ductile; at the yield condition the three specimens achieved a displacement of 5.7, 7.7, and 7.8 times the deflection measured at the maximum live load condition. Failure of the specimens was a shear compression failure (web shear) which occurred in the 4 in. thick web of the concrete T-sections; this occurred at an ultimate displacement of 10.8, 11.0, and 11.8 times the deflection measured at the maximum live load condition; after this ultimate displacement was reached, the load dropped by 25%, 29%, and 32% of its ultimate value.

The system shows promise for use in the modular prefabricated area of commercial construction. It has the potential to cut construction time, reduce the quantity

of materials used, and provide a cost effective solution for structural frames. This thesis outlines the results and analysis of the testing performed at the structures lab.

CHAPTER 2

SCOPE AND OBJECTIVES

This thesis consisted of the following research objectives:

1. Test the Plattform Building System specimens to failure to determine their elastic and ultimate capacity under gravity type loading conditions, as well as measure associated deflections.
2. Determine the code level of performance of the system.
3. Explore the appropriateness of analyzing the specimens using basic beam theory.
4. Develop a strut and tie model that predicts the behavior of the system and accounts for the large voids in the beam's web.
5. Determine the ability of the specimens to act as composite beams, and recommend potential design improvements

CHAPTER 3

TESTING PROGRAM

3.1 Test Specimens

The Plattforms test specimens were composed of a concrete T-section with mechanical openings cast onto a W10X12 with nelson studs and reinforcing bars welded to the top flange. The dimensions and connection layout can be seen in Figure 3.1. Supports for the testing were 6 in. wide tube steel. Concrete for the specimens consisted of light weight concrete with compressive strength on the day of the test of: $f_c' = 4950psi$. A 4X4-W2.0XW2.0 welded wire mesh was cast into the deck, all other reinforcing bars were #4. The overall dimensions of the specimens were as follows: length 13 ft., width 4 ft., and depth 2 ft-8 in. Bent plate steel, ¼ in. thick, was cast into the sides of the deck and reinforced with welded #4 bars and 2 in. nelson studs. Under normal conditions these plates would be used to attach double T spans to adjacent spans through welded connections. The steel used for the W10X12 was A992 steel with AISC code values for yield strength of F_y =50-65ksi, and ultimate strength of $F_u = 65ksi$.

3.2 Instrumentation

Each specimen was instrumented slightly differently, with additional strain gauges and LVDTs being applied as testing progressed. The final layout for strain gauges

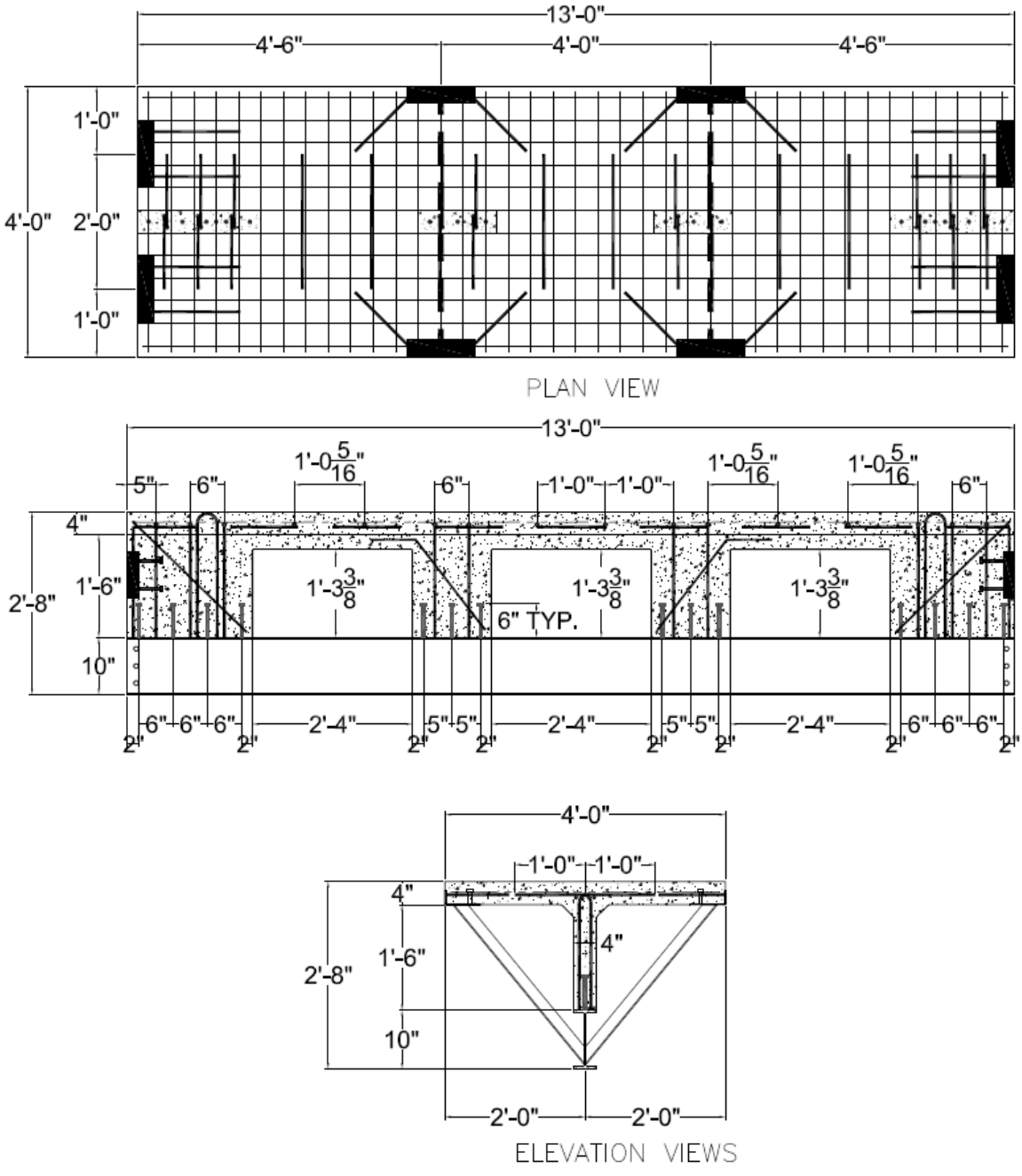

Figure 3.1: Specimen Layout

and LVDTs is shown in Figure 3.2. Strain gauges were used to measure micro strains at various locations on the steel beam, concrete web, and deck. LVDTs measured deflection at the bottom of the steel beam.

The first specimen was equipped with strain gauges 1-5, and 7-9, as well as LVDT 1 at the midspan of the beam. Strain gauges 1-4 were placed to measure strains resulting from shearing stresses near the support. Strain gauges 5 and 7 measured the strains resulting from flexure in the I-beams top and bottom flange respectively. LVDT 1 measured downward deflections at the midspan of the beam.

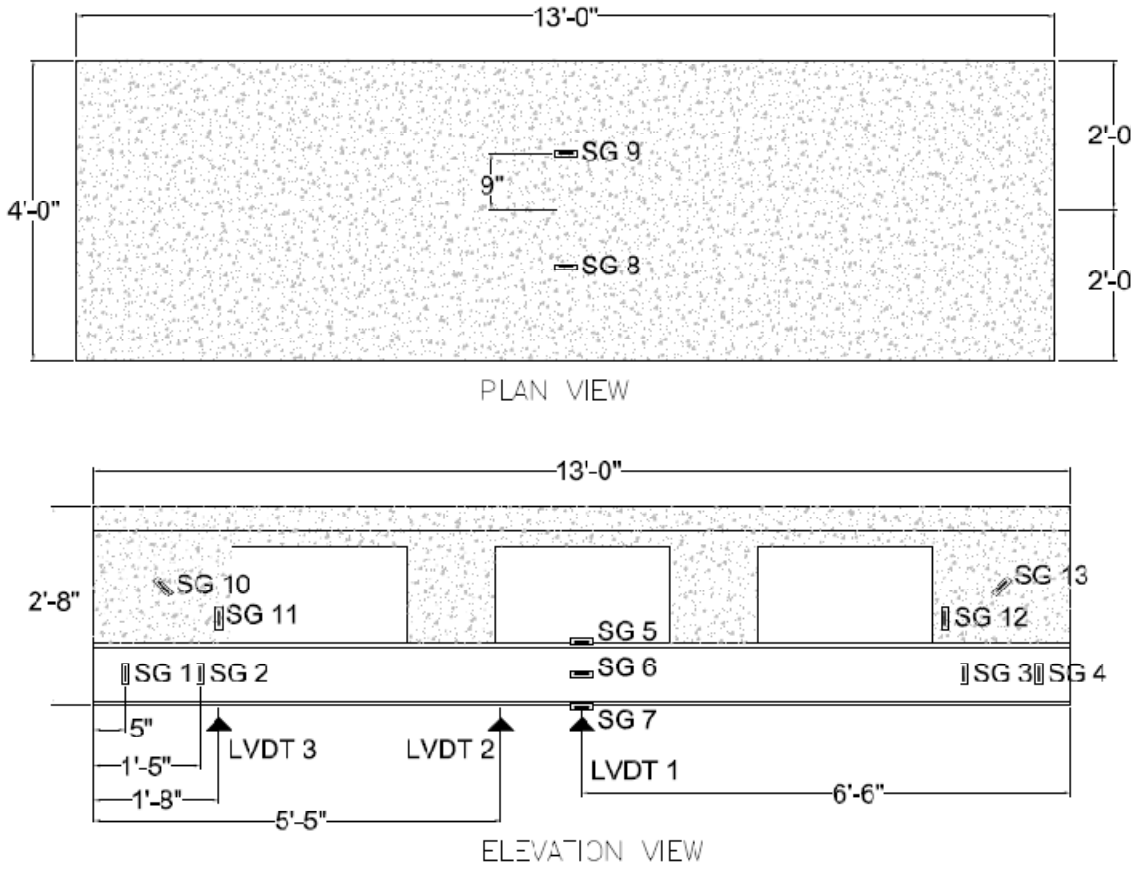

Figure 3.2: Instrumentation

The second specimen included all of the strain gauges and LVDTs as the first, with the addition of strain gauges 6, ll, and 12. It was observed in the first specimen that the top flange of the steel beam entered into compression while the bottom flange was in tension. This indicates that the steel beam was carrying load as a flexural member as opposed to a tension member in a fully composite system. Strain gauge 6 was added to gather more information regarding the location of the neutral axis of the system. Initial cracking of the first specimen occurred near strain gauge 11 and 12. These gauges were added to give insight into the web shear in the concrete end stem walls. LVDTs 2 and 3 were added to help graphically visualize the deflected shape of the beam with greater detail.

The third specimen included all of the previous strain gauges and LVDTs with the addition of strain gauges 10 and 13. Previous observation showed consistent failure in the end stem walls. Gauges 10 and 13 were added to further investigate the strain distribution that existed in the stem walls.

3.3 Loading Regime

Loading for all specimens was deflection controlled not exceeding 1/16 in. per minute. Load was transferred from a hydraulic piston to stiffened short span W-sections and then onto two 2 in. thick steel plates, 8 in. wide by 14 in. long, resting on the deck of the specimen. The loading pattern was designed to simulate the effects of a distributed load on the system. At the onset of loading, bending of the specimens resulted in load transfer to the outer steel plates only (thus for the first test the center plate did not serve any purpose in distributing load to the system). After the first test it was noted that

eccentric loading of the interior stem walls caused flexural cracks in the concrete web. This result was undesirable as it did not represent the effects of a symmetrically distributed load. Subsequent tests spread the load such that the load transferring steel plates were centered above the interior stem walls. A schematic drawing for the loading regime of the first specimen can be seen in Figure 3.3.

Loading for specimens 2 and 3 was identical to specimen 1, except that the load was applied closer to the center of the interior stem walls. Eccentricity, e, measured from the center of the interior stem walls to the application of the load was reduced from 7 in. to 1 ½ in. for the second and third tests in comparison to the first; this assumes the load can be approximated as a point load applied at either end of the stiffened loading beam. A schematic drawing for the loading regime of the second and third specimens can be seen in Figure 3.4.

The a/d ratio for the test specimens were 2.0 for the first test, and 1.8 for the second and third tests and can therefore be classified as short shear spans. Short shear spans are characterized by a/d ratios ranging from 1 to 2.5. During extreme loading they develop inclined cracks and, after a redistribution of internal forces, are able to carry additional load in part by arch action. The failure of such beams is generally caused by a bond failure, a splitting failure, a dowel failure along the tension reinforcement, or -as was observed in this case- a shear compression failure. Shear compression failures are characterized by crushing of the compression zone over the top of inclined shear cracks. Because the inclined crack generally extends higher into the beam than does a flexural crack, failure occurs at less than the flexural moment capacity (Wight & Macgregor 240).

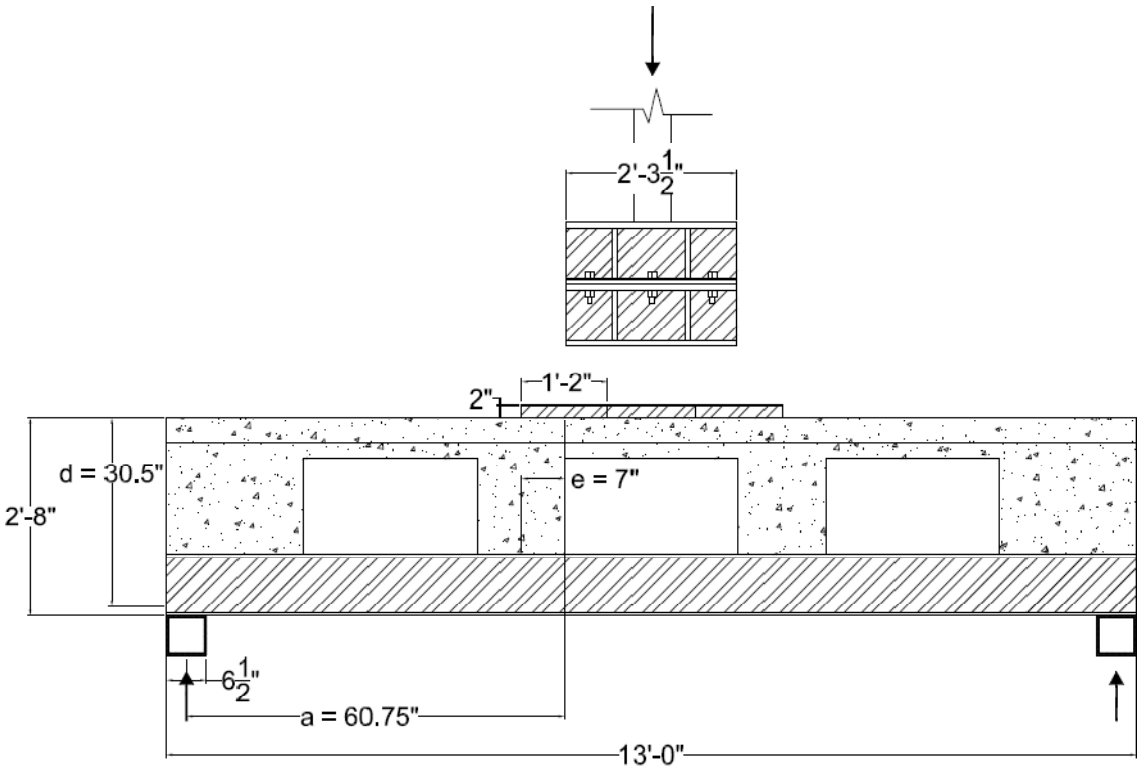

NORTH ELEVATION

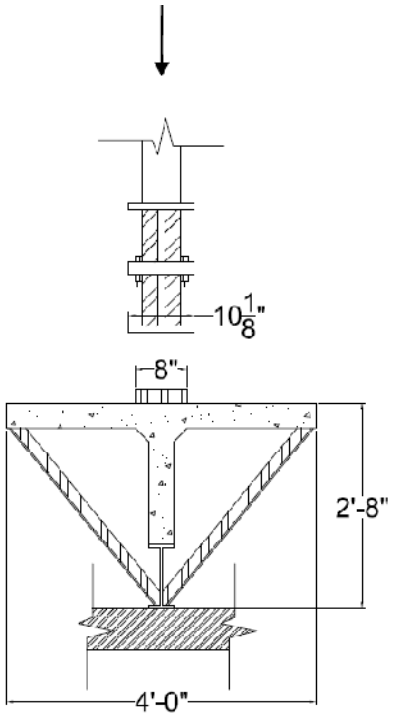

EAST ELEVATION

Figure 3.3: Specimen 1 Loading

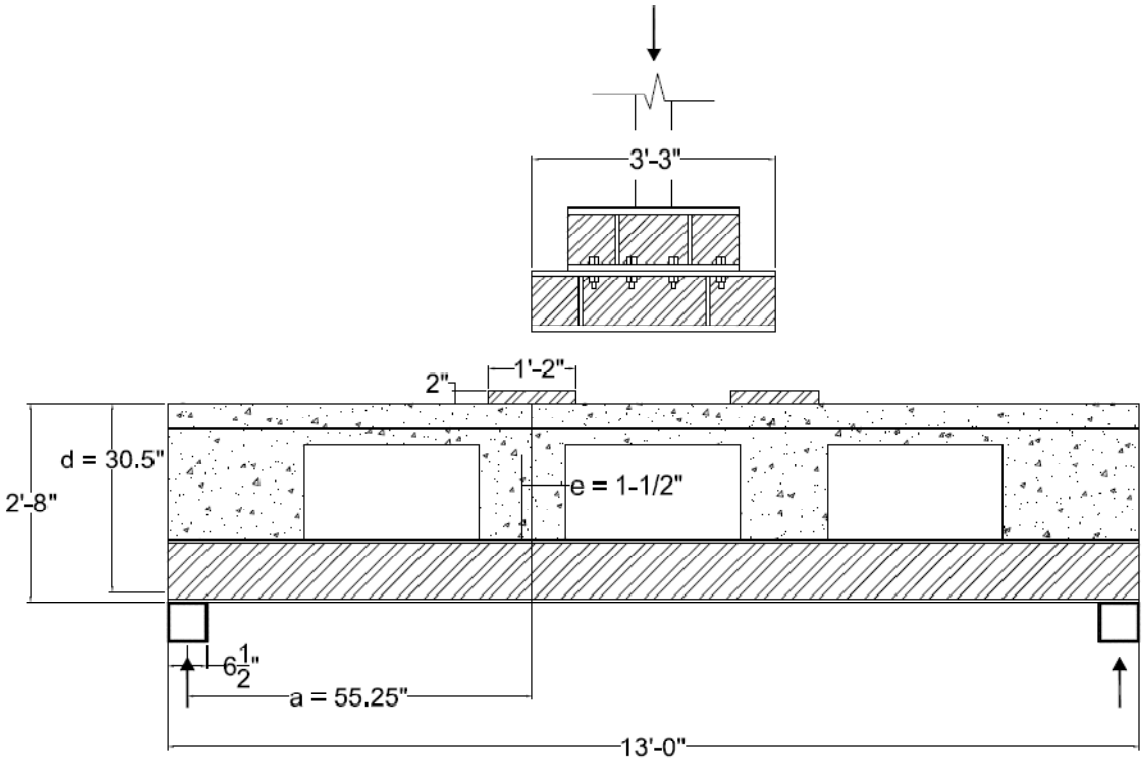

NORTH ELEVATION

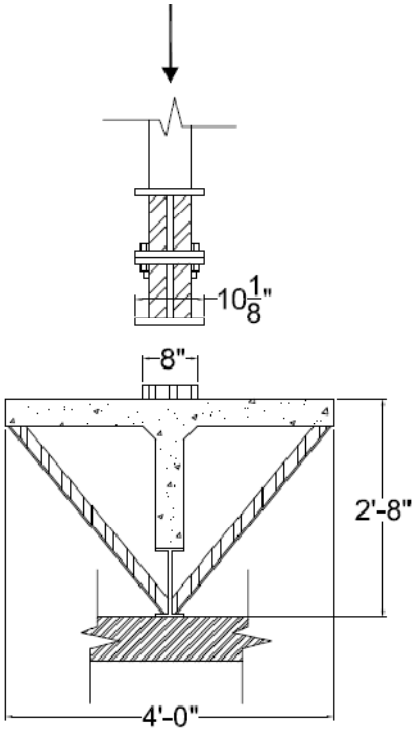

EAST ELEVATION

Figure 3.4: Specimen 2 and 3 Loading

CHAPTER 4

EXPERIMENTAL RESULTS

4.1 Load vs. Deflection

For code comparison the total load applied to the specimens was related to the effect of a distributed load on the system. This was done by simply dividing the total load by the area of the deck, and comparing it to ASCE 7 expected live loads for different applications. The worst case loading outlined in ASCE 7 consists of a distributed live load of 250 psf for heavy manufacturing or heavy storage warehouse applications. Using the equivalent effect of a distributed live load of 250 psf over the entire surface of the system, and a load factor of 1.6, the following is concluded: (1) the live load condition for heavy manufacturing or heavy storage warehouse applications falls well within the elastic portion of behavior of the system. At the point of nonlinear behavior of the tested spans, the system achieved a capacity of 4.3, 4.9, and 5.1 times the factored surface load, where the variability comes from the two different loading conditions; (2) the displacement at midspan was compared to the maximum permissible deflections in ACI 318 for the three specimens. It was found to reach only 15% of the allowable for floors supporting nonstructural elements not likely to be damaged by large deflections (L/240) to 30% of the allowable for floors supporting nonstructural elements likely to be damaged by large deflections (L/480).

At the point of nonlinearity the three specimens achieved a displacement of 5.7, 7.7, and 7.8 times the deflection measured at the factored surface load. Failure of the specimens was a shear compression failure (web shear) which occurred in the 4 in. thick web of the concrete T-sections; this occurred at an ultimate displacement of 10.8, 11.0, and 11.8 times the deflection measured at the factored surface load; immediately after this ultimate displacement was reached, the load dropped by 25%, 29%, and 32% of its ultimate value as seen in Figure 4.1.

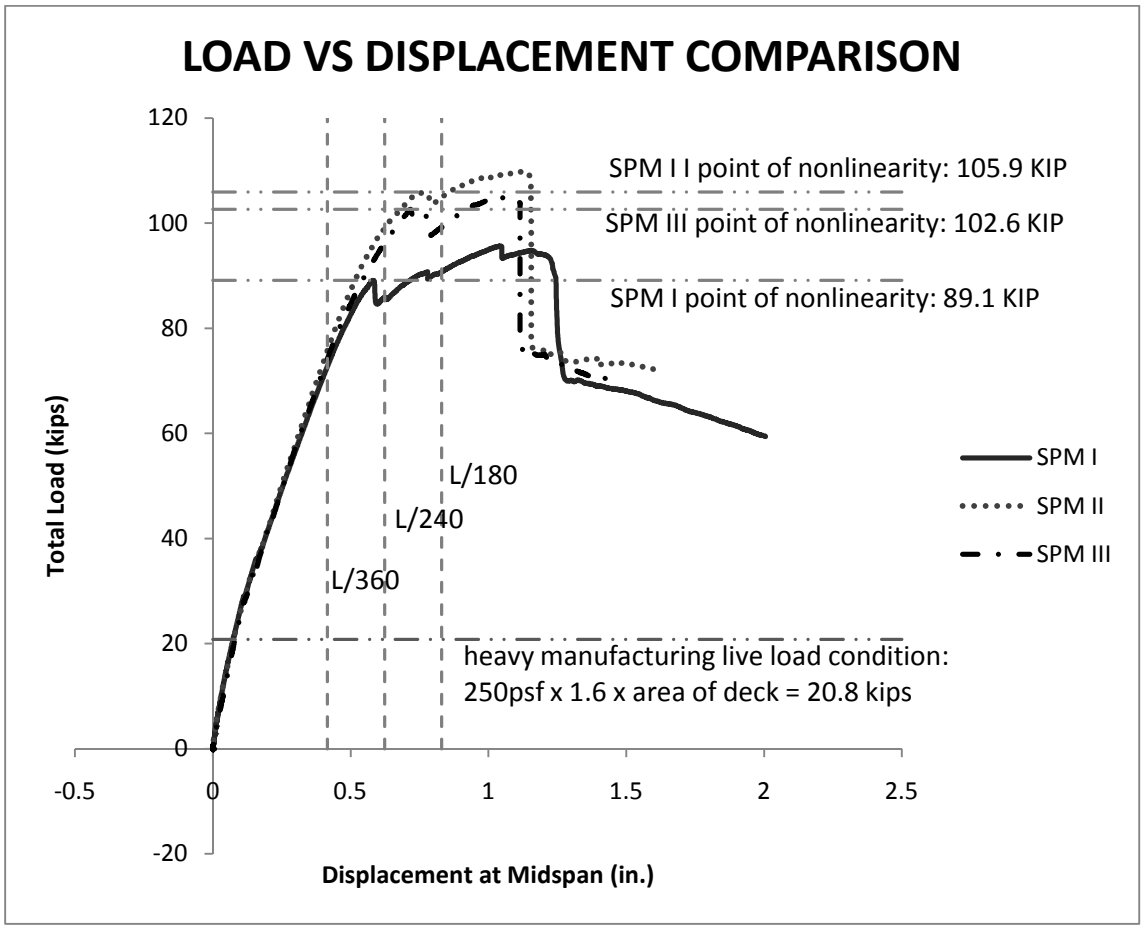

Figure 4.1: Load vs. Displacement Comparison

4.2 Displaced Shape

The curves representing the measured displacement along the member, shown in Figure 4.2, provide insight to what the moment diagram for the system looks like. The shape drawn by three points along the base of the beam demonstrate the stiffening effect that the end stem walls have in restraining the moment. This can also be seen in Figure 4.3. For a simply supported beam we would generally expect a more parabolic shape. The deflection increases slowly at first with substantial load increase, then progresses rapidly beyond the ultimate load condition. The final deflection is representative of the system after a 30% decrease in load compared to the ultimate load condition.

4.3 Location of Neutral Axis

The location of the neutral axis for each specimen was estimated based on strain compatibility for the yield and ultimate conditions. The neutral axis was estimated as the distance from the bottom flange where a line joining strain crosses the vertical axis as shown in Figure 4.4. The location of the neutral axis was estimated at 6.83 in., 7.79 in., and 7.64 in. for the first second and third specimens, respectively. The location for the first specimen likely varies from the other two because of the different loading conditions.

Tests two and three included an additional strain gauge at the mid-height of the steel web. The additional gauge provides further information for estimating the location of the neutral axis. It should also be noted that the low tensile strain at the ultimate load of specimen II is likely the result of a strain gage malfunction, in which the strain gage

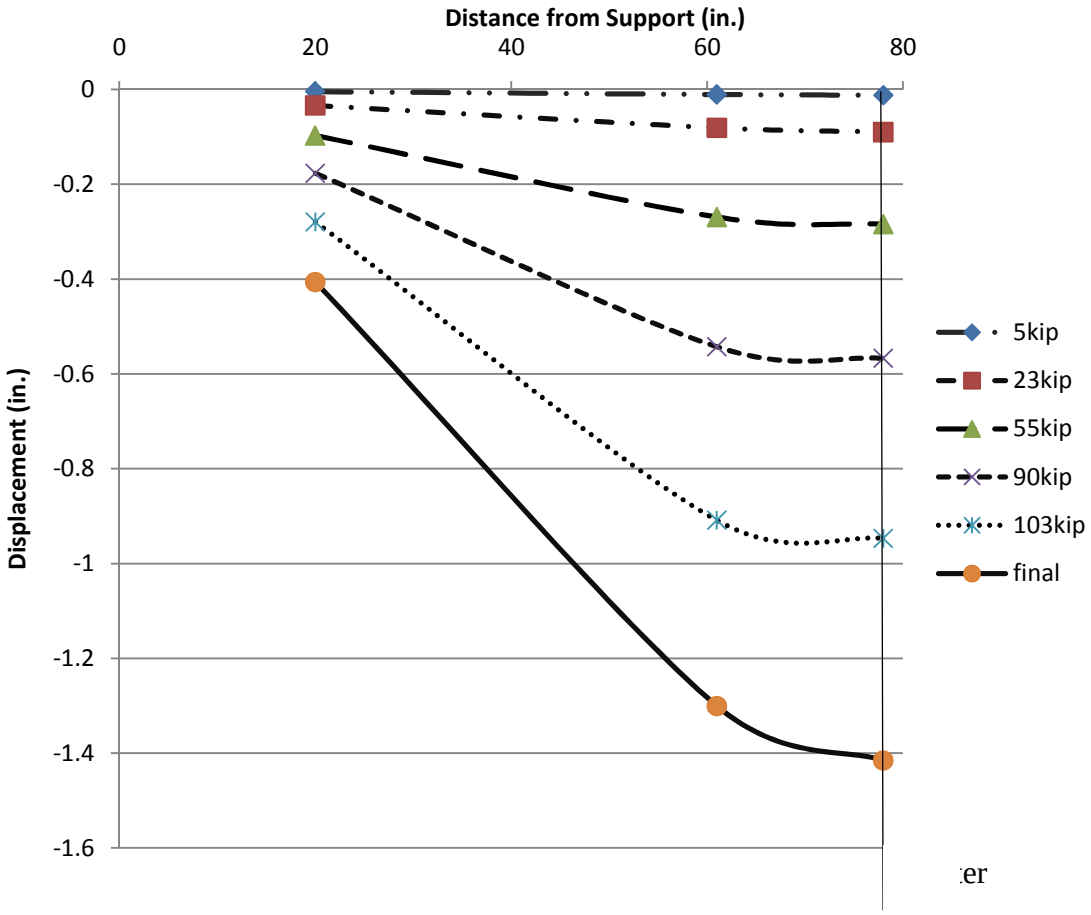

Figure 4.2: Specimen III Displaced Shape

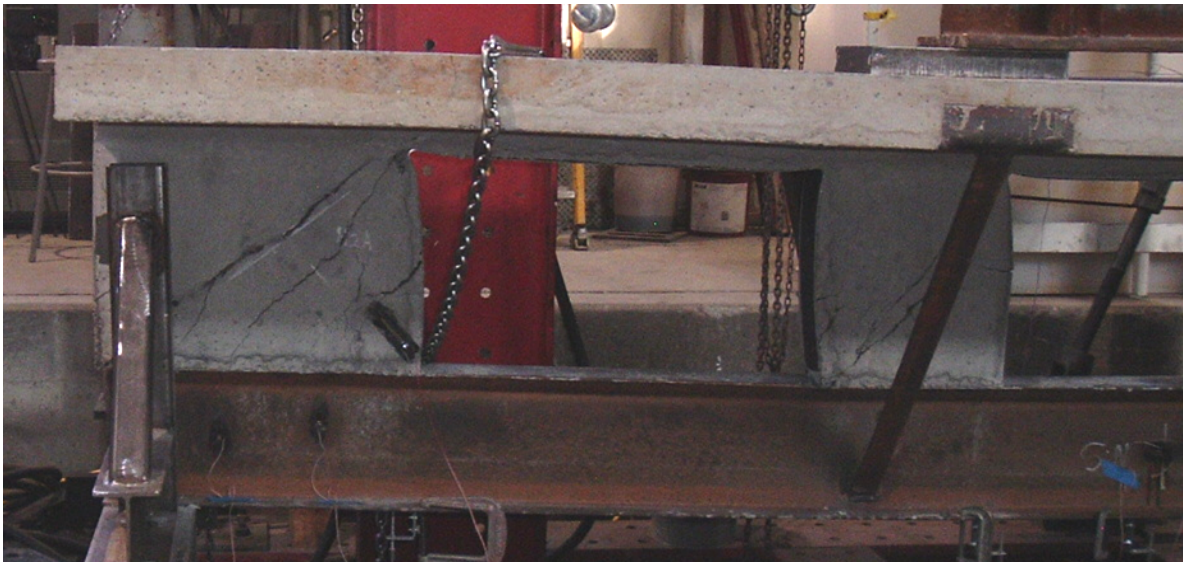

Figure 4.3 Picture of Displaced Shape

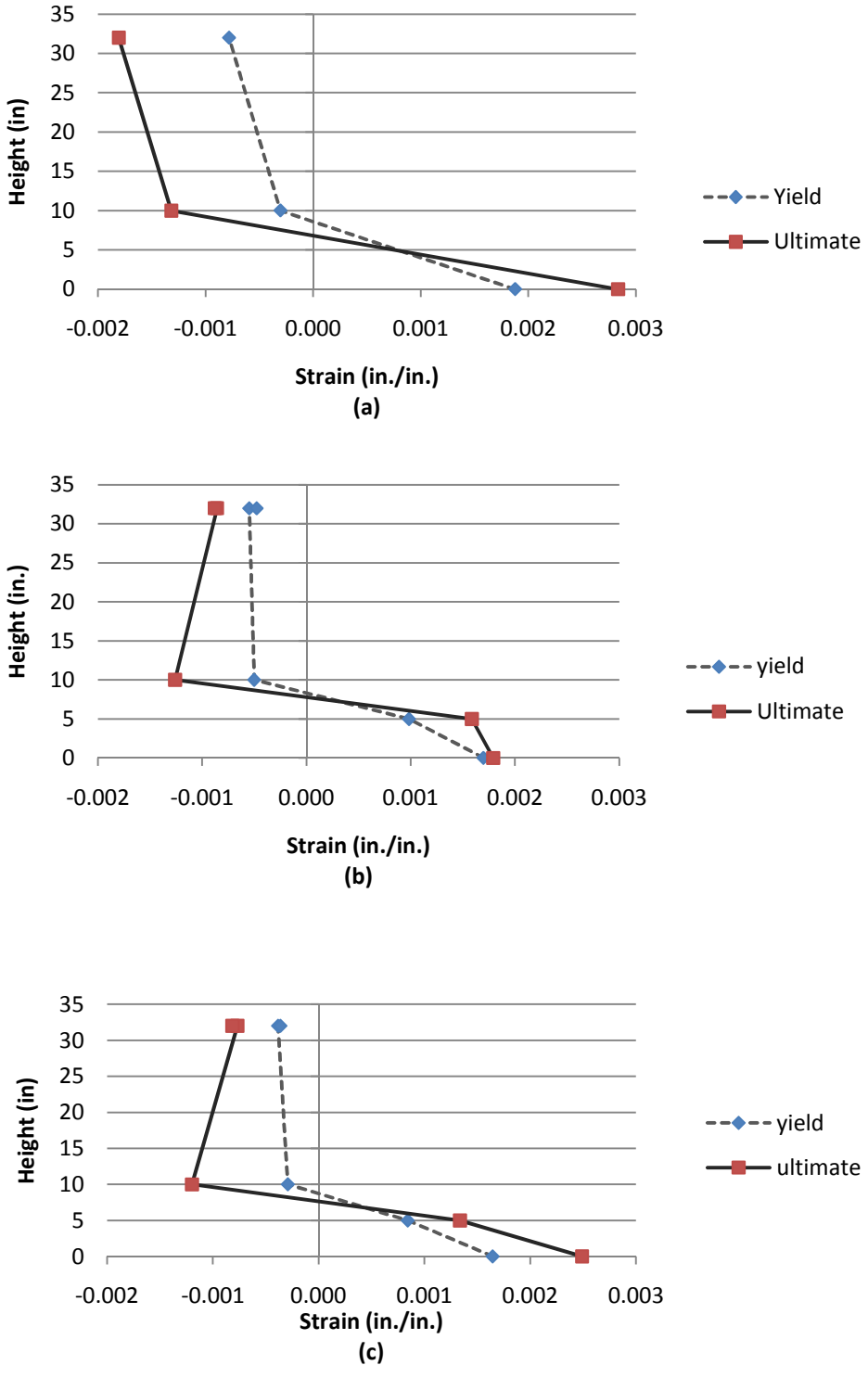

Figure 4.4: Location of Neutral Axis Plots and Horizontal Strain at Midspan: (a) SPM I, (b) SPM II, and (c) SPM III

lost adhesion to the bottom surface of the steel beam. However the other three strain gauges still give a good estimation for the location of the neutral axis of the specimen.

The location of the neutral axis in the web of the steel beam demonstrates that the specimens never acted as fully composite members. In order for this system to be truly composite the steel would have to be entirely in tension with the neutral axis located somewhere in the T-section of the concrete. Instead the test specimens always exhibited flexural bending in the steel beam. It would be expected that the system would have higher flexural strength if it were able to perform as a composite member.

CHAPTER 5

ANALYTICAL RESULTS

5.1 Flexural Analysis

For flexural analysis, the theoretical bending moment diagrams at ultimate loading for each specimen were plotted assuming four-point loading with the forces from the loading device centered in the middle of the steel load transferring plates as shown in Figure 5.1. The distance along the x-axis of the moment diagrams represents the span length from center of support to center of support

5.2 Theoretical Flexural Analysis

The theoretical flexural analysis is limited by because it was observed that the specimens failed in shear before reaching their flexural moment capacity. The analysis is therefore based on observed strains from the third test specimen. The third specimen was chosen because it had more strain gauges at the midspan of the steel beam to measure longitudinal strains than the first specimen, and unlike the second specimen there were no issues with possible adhesion loss of strain gauges.

The analysis follows a similar procedure as employed when analyzing a concrete T-beam with tensile steel reinforcement. The theory for this analysis is based on statics where forces in a beam are resisted by internal moments, and the largest internal moment

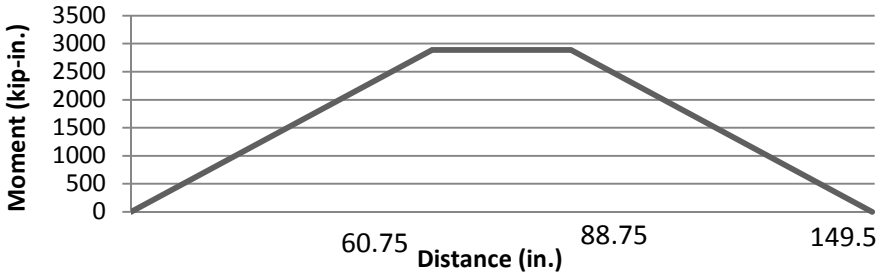

(a)

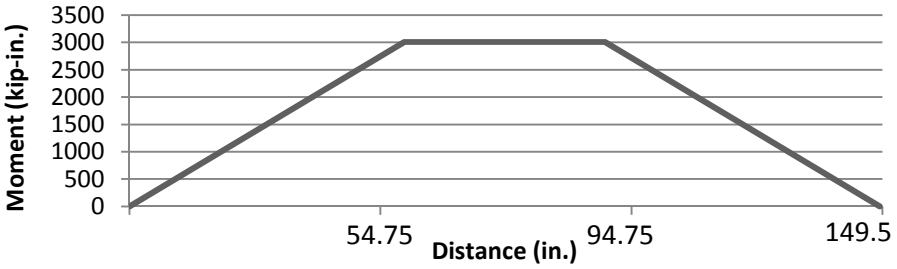

(b)

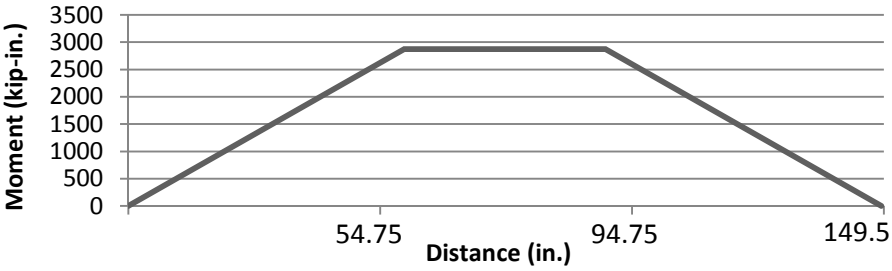

(c)

Figure 5.1: Moment Diagrams: (a) SPM I, (b) SPM II, (c) SPM III

for a simply supported beam under evenly distributed loading will occur at midspan. Therefore the maximum moment experienced by the beam should equal the tensile force in the steel multiplied by the distance between the centroid of the tensile and compressive forces.

It was assumed that the stress block for the concrete was largely rectangular; this is supported by the nearly vertical slope of the lines between the uppermost strain gauges in Figure 4.4. The steel mesh in the top deck was not taken into consideration for the compressive strength of the deck because it was in the compression block. The stress in the steel is based on the observed strains, where stress equals strain multiplied by the modulus of steel, except where strains have gone beyond yielding for which stress is limited to 65ksi. The tensile and compressive forces and centroids of the tensile and compressive stress distributions were obtained through a weighted area averaging method using the strains of Figure 4.4, an ultimate stress of 65ksi, and a modulus of steel of 29000ksi. The results of this approach are shown in Table 5-1 and Table 5-2 for tensile and compressive force distributions respectively.

To summarize Tables 5-1 and 5-2, the height was measured from the base of the steel beam in the vertical direction. Stress was computed at each height increment using the strain inferred by Figure 4.4 multiplied by the modulus of steel (29000 ksi). The area was computed using the dimensions of the steel beam, and the height bounds of the current and subsequent rows in the tables. The average stress was computed by averaging the stress from the current and subsequent row. The average force was computed by multiplying the average stress by the average area. The centroid column was computed as the center of mass of a trapezoid formed by the strains inferred from Figure 4.4 and

Table 5-1: Tensile Force in Steel Beam Based on Observed Strains

height (in.)	stress (ksi.)	area (in.^2)	average stress (ksi)	average force (kips)	centroid (in)	force X centroid (kip x in.)
0.00	65.00	0.40	65.00	25.74	0.05	1.29
0.10	65.00	0.44	65.00	28.31	0.16	4.39
0.21	65.00	0.20	65.00	12.82	0.32	4.16
0.51	65.00	0.06	65.00	3.71	0.66	2.45
0.81	65.00	0.06	64.89	3.70	0.96	3.55
1.11	64.78	0.06	63.78	3.64	1.26	4.58
1.41	62.78	0.06	61.77	3.52	1.56	5.49
1.71	60.77	0.06	59.76	3.41	1.86	6.33
2.01	58.76	0.06	57.75	3.29	2.16	7.11
2.31	56.75	0.06	55.75	3.18	2.46	7.81
2.61	54.74	0.06	53.74	3.06	2.76	8.45
2.91	52.73	0.06	51.73	2.95	3.06	9.02
3.21	50.73	0.06	49.72	2.83	3.36	9.52
3.51	48.72	0.06	47.71	2.72	3.66	9.95
3.81	46.71	0.06	45.70	2.61	3.96	10.31
4.11	44.70	0.06	43.70	2.49	4.26	10.61
4.41	42.69	0.06	41.69	2.38	4.56	10.83
4.71	40.68	0.06	39.64	2.26	4.86	10.98
5.01	38.60	0.06	36.39	2.07	5.16	10.70
5.31	34.19	0.06	31.98	1.82	5.46	9.95
5.61	29.78	0.06	27.58	1.57	5.76	9.05
5.91	25.37	0.06	23.17	1.32	6.06	8.00
6.21	20.97	0.06	18.76	1.07	6.35	6.80
6.51	16.56	0.06	14.36	0.82	6.65	5.44
6.81	12.15	0.06	9.95	0.57	6.95	3.94
7.11	7.75	0.06	5.54	0.32	7.24	2.29
7.41	3.34	0.06	1.67	0.10	7.51	0.71
7.71			summation	122.26	kips	183.70 kip x in.
			centroid	1.50	In.	

dependent on the distribution of steel area within the bounded heights. The total force was determined by adding all of the average forces for each area. The centroid was computed as a weighted average based on the sum of the forces and centroids of each layer multiplied together, divided by the total force. It was thereby deduced that the total tensile force developed during testing of the third specimen was 122.26 kips centered 1.5 in. from the base of the steel beam. The compressive force in the steel beam was 38.19 kips centered 9.73 in. up from the steel beam. Figure 5.2 shows the equivalent forces and centroids graphically. This leaves an unresolved compressive force of 84.07 kips to be carried by the concrete flange. Knowing the amount of force carried by the concrete allows us to calculate the depth of the compression zone in the concrete (α).

$$\alpha = \frac{unresolved\ compressive\ force}{0.85 \cdot f_c' \cdot b_e}$$

$$b_e \leq \begin{cases} transverse\ span \\ b_w + 2 \cdot (8 \cdot h_f) \\ l/4 \end{cases}$$

$$h_f = depth\ of\ concrete\ flange$$

From the above equations α was calculated as 0.51 in. Assuming the concrete compressive force acts at the center of the compression block, it is now possible to determine the resultant compressive force and its line of action. This is done by taking a weighted average of the compressive forces in the concrete and steel at their lines of action. The compressive force, adequate to resist the tension in the steel beam, acts at a centroid 24.87 in. from the base of the beam. This is shown in Figure 5.2. Next the moment is calculated by multiplying the total tensile force by d, resulting in a moment of 2,857 kip-in. This calculated moment, using strains measured from specimen III, is less than 1% different from the observed moment of specimen III.

Table 5-2: Compressive Force in Steel Beam Based on Observed Strains

height (in.)	stress (ksi)	area (In.^2)	average stress (ksi)	average force (kips)	centroid (in.)	force X centroid (kip x in.)
10.00	34.71	0.40	33.98	13.45	9.95	133.87
9.90	33.24	0.44	32.43	14.13	9.85	139.09
9.79	31.63	0.20	29.42	5.80	9.68	56.15
9.49	27.22	0.06	25.01	1.43	9.34	13.32
9.19	22.81	0.06	20.61	1.17	9.04	10.62
8.89	18.40	0.06	16.20	0.92	8.74	8.07
8.59	14.00	0.06	11.79	0.67	8.44	5.67
8.29	9.59	0.06	7.39	0.42	8.14	3.43
7.99	5.18	0.06	2.98	0.17	7.84	1.33
7.69	0.78	0.06	0.39	0.02	7.54	0.17
7.39			summation	38.19	kips	371.72 kip x in.
			centroid	9.73	In.	

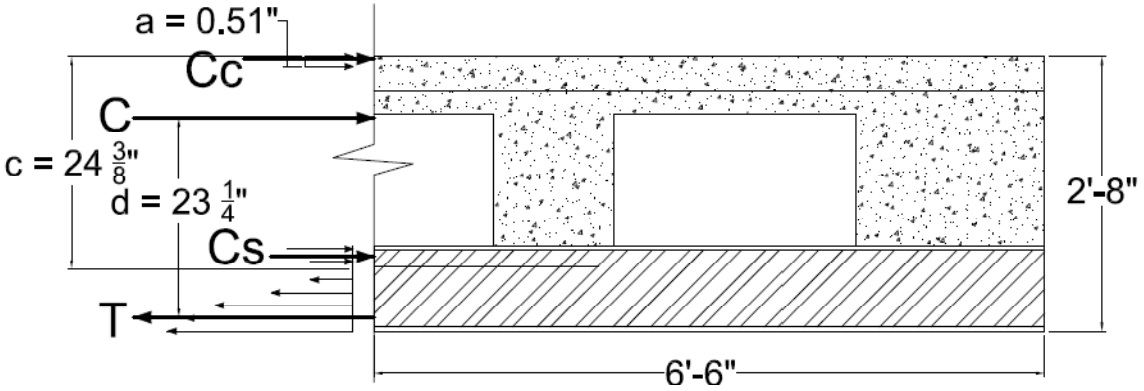

Figure 5.2: Theoretical Stress Distribution

It is impossible to determine the true moment capacity of the specimens because they all failed in shear compression. It should be noted that the inability of the system to achieve full composite action also limits the flexural capacity, because the steel is not allowed to fully plastify.

5.3 Shear Analysis

The shear analysis assumed the same four-point loading as the flexural analysis and the shear diagrams for each specimen can be seen in Figure 5.3. Again the span is taken as the distance from center of support to center of support. The imposed loading is assumed to be a point load acting at the center of the steel load transfer plate on the concrete deck.

5.4 Theoretical Shear Analysis

The shear analysis presented in this thesis is focused primarily on the shear capacity of the concrete web of the test specimens. This is because test observations showed that this is where shear compression failure occurred. Further, the steel beam has a code listed shear strength of $\varphi V_n = 56.3$ kips, this is based on f_y = 50 ksi and is likely to be exceeded in actual tests. With reactions measuring in the 50 kip range it is clear that the steel beam will be capable of carrying the induced shear load, again it is the concrete web that is of interest. The shear capacity is made up of the shear contribution from the steel bars and concrete T-section.

The concrete web is not continuous and the mechanical openings in the web are so large that the entire beam is considered a discontinuity region. For such regions beam

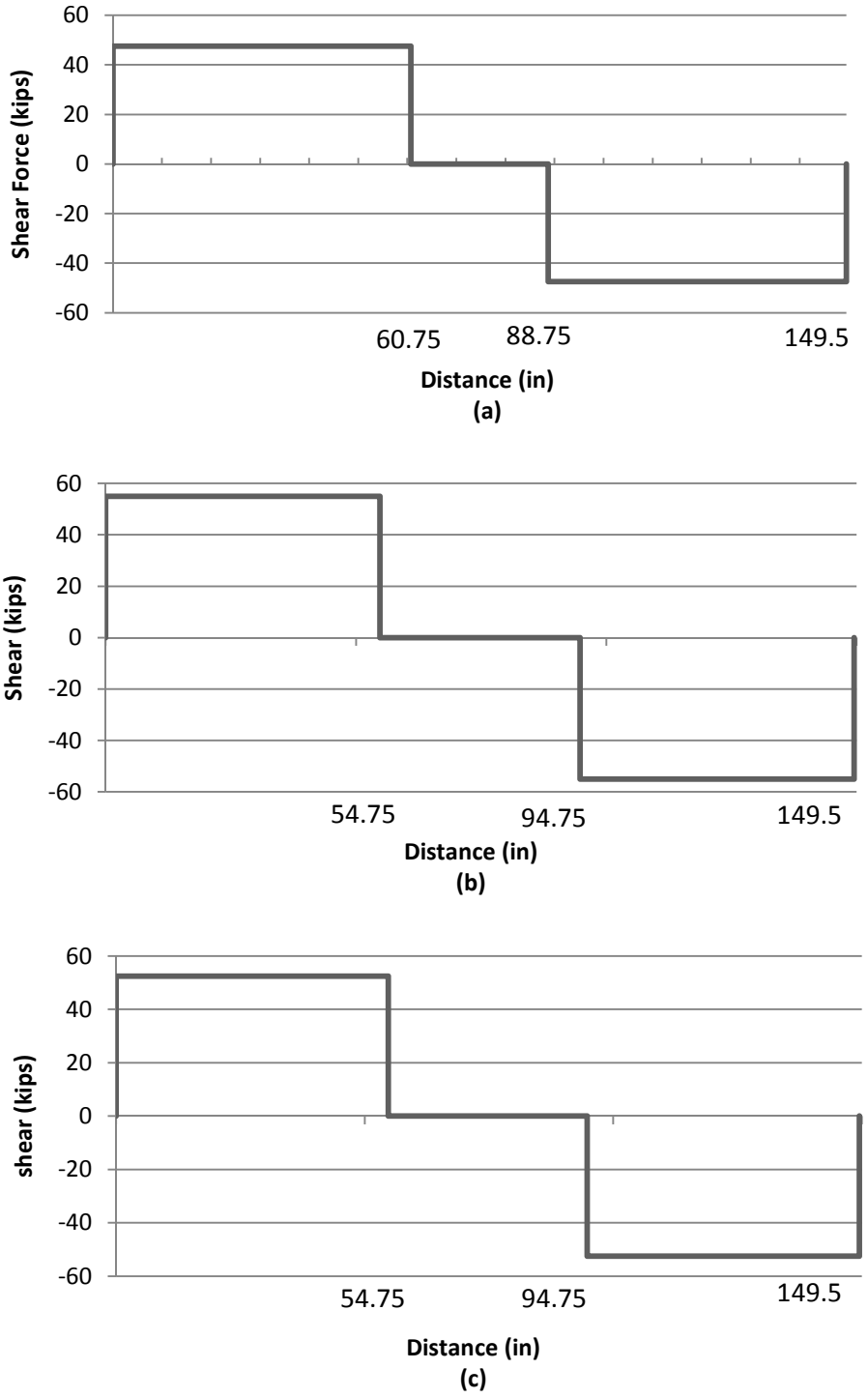

Figure 5.3: Theoretical Shear Diagrams: (a) SPM I, (b) SPM II, (c) SPM III

theory does not apply and a method such as a strut and tie model or finite element analysis should be used to determine the theoretical shear capacity of the specimens. This thesis presents a strut and tie model in Chapter 6 to analyze the specimens.

CHAPTER 6

COMPOSITE BEHAVIOR

St. Venant's principle indicates that discontinuity occurs in the stress distribution of a structural element at changes in geometry or at concentrated loads and reactions. Such discontinuities are typically assumed to extend a distance, ***h***, equal to the overall height of the member from the section where the load or change in geometry occurs, and are typically labeled D-regions. In D-regions beam theory does not apply and either finite-element analysis or a strut-and-tie model is required for analysis (Wight & Macgregor 841). The Plattforms building system is characterized by large closely spaced mechanical openings in the concrete web, such that the entire member is classified a D-region. This thesis applies a simple strut and tie model to the system using idealized prismatic compression struts in the concrete and steel where applicable.

6.1 Strut and Tie Model

The strut and tie model, for the specimens, consists of prismatic struts, tension ties, and nodes. Figure 6.1shows the strut and tie load paths based on the location of the loading plates, reactions, and steel reinforcement in the test specimens. The load paths are symmetric about a vertical line passing through the specimen midspans. This results in equal forces being transferred to each of the reactions. Figure 6.2 shows the required

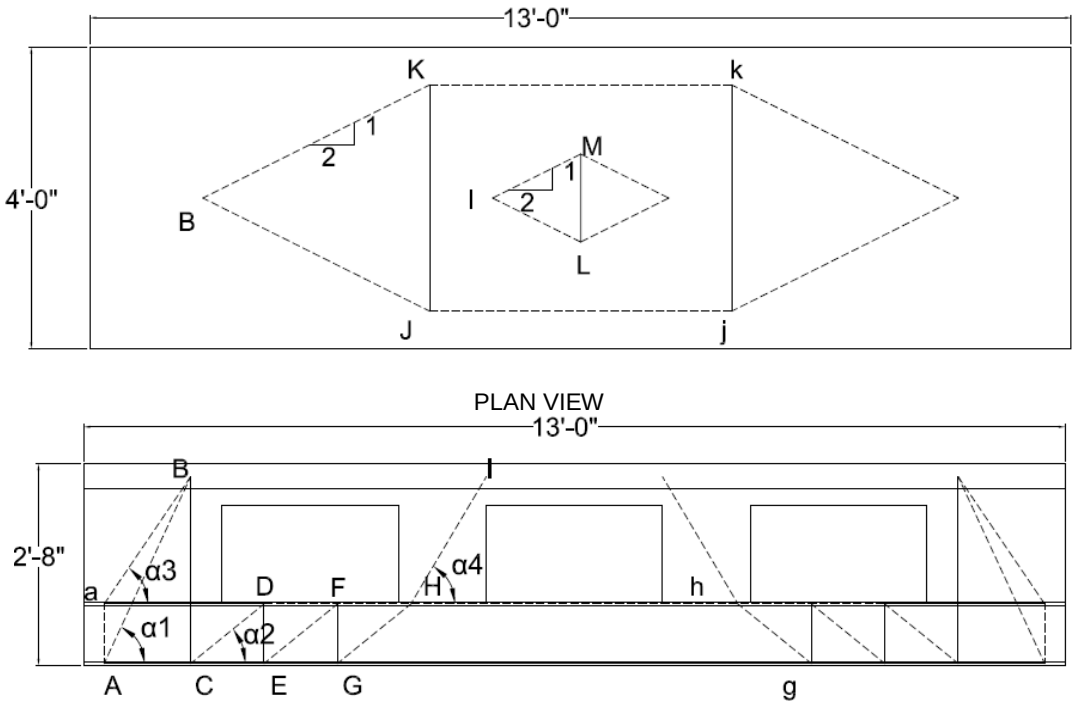

Figure 6.1:Three Dimentional Strut and Tie Load Paths

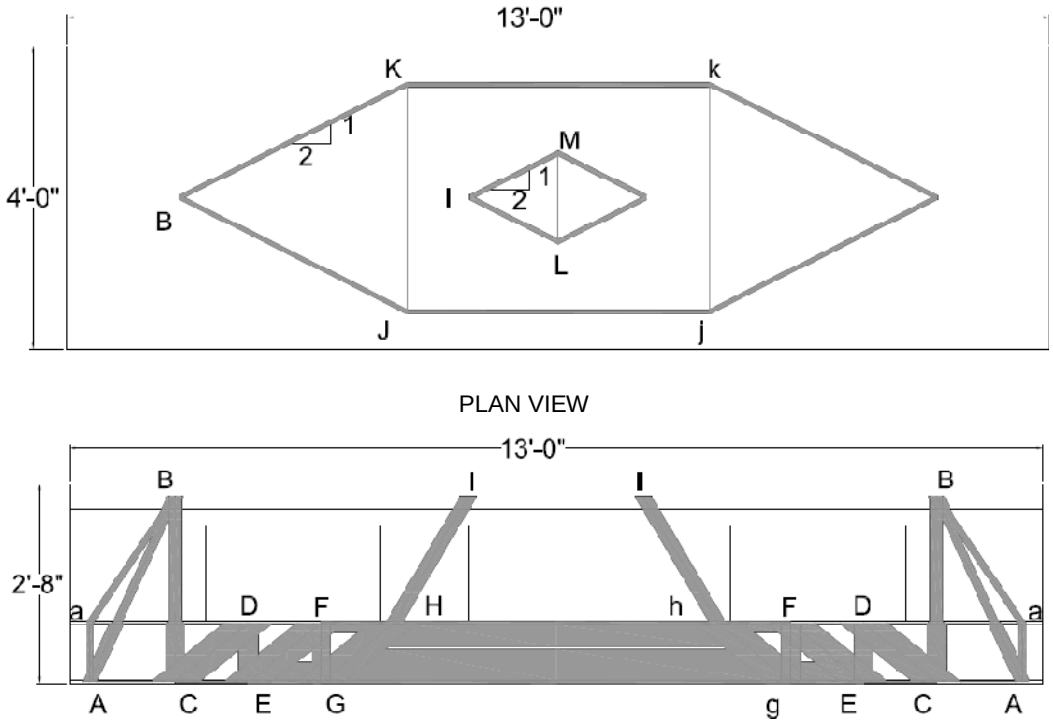

Figure 6.2: Geometric Requirements for Strut and Tie Model

widths for each of the struts as well as the depth of steel required in the W10X12 steel portion of the specimens.

The loading of the model was incrementally increased until the geometric constraints of the specimen made it impossible for the struts and ties to transfer load, and the model failed. This occurred first at a load where compression strut Hh (longitudinal tension in the steel beam at and near midspan) and tension tie Gg (longitudinal compression in the steel beam at midspan) began to overlap. This flexure type failure of the steel beam is not representative of the observed behavior of the system which failed in shear compression and was characterized by large shear cracks in the concrete stem walls.

The model accounted for a concrete strength reduction of $0.75f_c'$ for the effect of biaxial compression on the web using equations proposed by Vecchio and Collins, where f_2 represents the reduced compressive strength of the concrete:

$$f_2 = f_{2max}\left[2\left(\frac{\varepsilon_2}{\varepsilon_c'}\right) - \left(\frac{\varepsilon_2}{\varepsilon_c'}\right)^2\right]$$ (Vecchio and Collins, 224)

where:

$$f_{2max} = \frac{f_c'}{0.8 + 170\varepsilon_1} \leq f_c'$$

and:

$\varepsilon_1 = 0.0012$ assumed

$\varepsilon_2 = 0.002$ assumed

$\varepsilon_c' = 0.003$ assumed

Even with the reduction in concrete strength the model still did not accurately predict the mode of failure of the specimens. Additional considerations include the

assumption that the concrete could support compressive loads along the steep paths proposed by the model within the stem walls. Had shallower angles, closer to the ideal 45^{o}, been used the model would have failed those compression struts much sooner as they began to overlap the open space of the mechanical openings. Also per Figure 3.1, some tensile reinforcement was provided; however to improve the shear capacity of the specimens would require either a thicker concrete web or increased concrete confinement. It was also clear in testing that tension tie BC in Figure 6.1 would be more effective if the vertical reinforcing were placed closer to the mechanical block out.

One of the strengths of this model is the proposed load paths. These show that under the current design it is impossible for load to make it from the concrete deck to the reactions without resulting in compression in the steel beam. Without radical changes to the size and placement of the mechanical openings it is impossible for the system to maintain true composite behavior where the steel beam can be treated as a tension member only. The model also shows how flexural bending of the steel beam has the potential to further weaken the system, especially because this is where the model failed.

6.2 Numerical Results of Strut and Tie Model

The strut and tie numerical analysis is based in simple trigonometric calculations of force equilibrium for each node (see Appendix for their derivation). Table 6-1 gives a summary of the forces in the strut and tie model at failure. Areas and thicknesses of struts and ties are computed using material properties such as yield strength of steel and compressive strength of concrete. The steel beam was assumed to have a tensile and compressive strength of 65 ksi, this on the high extreme of the design range for A992

Table 6-1: Forces Summary

strut/tie	Force (kips)	tension/compression	strut/tie	Force (kips)	tension/compression
AB	20.49	compression	CE	46.75	tension
Aa	12.40	compression	EG	84.90	tension
aB	14.98	compression	Gg	123.05	tension
BC	31.00	tension	aD	8.41	compression
CD	49.16	compression	DF	29.74	compression
DE	31.00	tension	FH	67.89	compression
EF	49.16	compression	Hh	106.04	compression
FG	31.00	tension	BJ	9.51	compression
GH	49.16	compression	JK	4.25	tension
HI	36.03	compression	IM	10.26	compression
AC	8.60	tension	LM	4.59	tension

steel per AISC 13, for real world testing it is likely that the steel beam met or exceeded the proposed yield strength. The compressive strength of the concrete was measured on the day of testing at 4950 psi.

6.3 Observed Strut and Tie Formation

During the testing performed at the University of Utah patterns in the cracking and failure of all three specimens lend support to the strut and tie model outlined in this paper. Figure 6.3 shows typical cracking observed in the end stem wall of the specimen. The first signs of cracking appeared in the bottom right corner in the vicinity of strain gauge 11. As tension developed in the neilson stud in that corner it was unable to transfer into the concrete and cracking occurred until the reinforcing bars to the immediate left were able to support the tensile loads as shown in the proposed strut and tie model. Later cracking appeared along the lines closely corresponding to struts aB, and AB in Figure 6.1.

Figure 6.4 shows typical cracking of an interior stem wall after the loose and crushed concrete had been pried away. This cracking supports the formation of the strut HI in Figure 6.1. Some of the interior reinforcing is also visible in this figure, with a neilson stud in the lower left-hand corner, and number four reinforcing bars visible on either side of the stem wall.

It can be seen in these pictures that the inclined cracking of the stem walls follow much more shallow angles than proposed in the strut and tie model. This may be the primary reason why the strut and tie model does not capture the shear compression failure in the concrete web, where for shallower inclines the struts enter the hollow region of the mechanical openings. Future design considerations may include placing reinforcement closer to the mechanical opening to form a tension tie at a greater distance from the support, allowing for shallower inclines of struts in that region. Also the interior stem walls might be increased in width to allow for similarly shallow inclines.

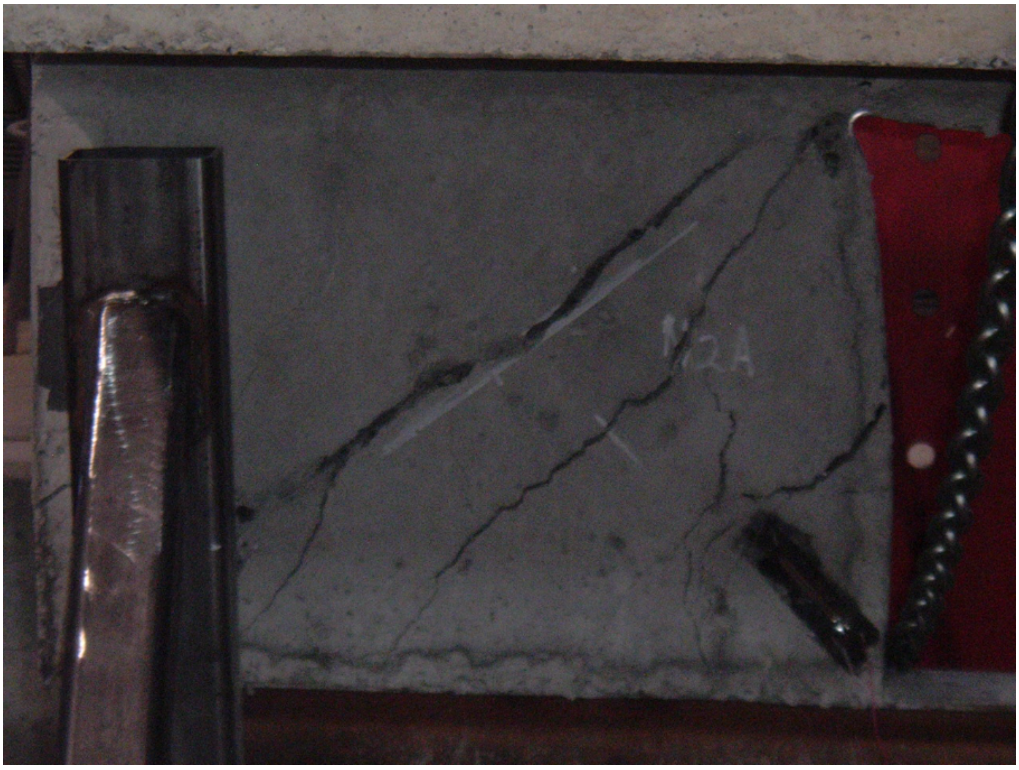

Figure 6.3: Typical Cracking of End Stem Wall

Figure 6.4: Cracking of Center Stem Wall SPM II

CHAPTER 7

DISCUSSION OF EXPERIMENTAL AND ANALYTICAL RESULTS

Table 7-1 shows the results of the Plattforms Building System tests. Where the load versus displacement curve became nonlinear loads ranged from 89 kips to 106 kips with point of nonlinearity displacements ranging from 0.55 to 0.74 in. The ultimate load climbed to a range from 96 kips to 110 kips with approximately 1 in deflections. Failure did not occur until the system displaced over an inch, however the system was still capable of maintaining a residual load of above 60 kips, equating to a 1.15 ksf live load on the deck.

Table 7-1: Summary Results

	Summary Table				
	Point of Nonlinearity Data		Ultimate Data		Ultimate Displacement
	Nonlin Load (kips)	Nonlin Disp. (in.)	Ult. Load (kips)	Disp. at Ult. Load (in.)	Disp (in.)
SPM I	89.1	0.546	95.6	1.023	1.21
SPM II	105.9	0.744	109.8	1.117	1.12
SPM III	102.6	0.735	105	1.05	1.09

Table 7-2 shows the observed capacity of each specimen, because the specimens failed in web shear the maximum moments represent only the observed moment at failure, the moment capacity could not be experimentally determined. Shear capacities ranged from 47.5 kips to 55 kips.

The theoretical analysis for both the flexure and shear of the system in the analytical results section are based on the application of beam theory to the composite system, similar to that of a reinforced concrete T-beams. The strut and tie model offers considerably greater insight into the behavior of the system and illustrates the load paths within the system. It shows that under the current layout composite behavior cannot be maintained. The model is conservative predicting the system's capacity at 62% of the observed value. This is because strut and tie models are design tools and are meant to be conservative, also the flexural behavior of the steel beam, requiring both tensile and compressive forces to develop in the cross-section, further limit the model. Further analysis coupled with improving the strut and tie model should show the usefulness of the model presented as a pattern for analyzing varying spans and dimensions of the Plattforms Building System.

Table 7-2: Observed Capacities

	Max. Moment (kip-in.)	Max. Shear (kips)	Height of Neutral Axis (in.)
Specimen I	2885.6	47.5	6.83
Specimen II	3011.3	55	7.79
Specimen III	2874.4	52.5	7.64

It was observed that the specimens failed in shear compression in the concrete web. This is to be expected for short shear spans such as the specimens tested. However the system does have potential for increased shear capacity through more efficient placement of reinforcement and better confinement of the concrete in the web area.

CHAPTER 8

CONCLUSIONS

1. The Plattform Building System specimens were tested to failure to determine their yield and ultimate capacity under gravity type loading conditions. The specimens yielded between 89 kips and 106 kips with ultimate loads ranging between 96 and 110 kips. Yield displacements ranged from 0.55 to 0.74 in. Failure did not occur until the system displaced over an inch, however the system was still capable of maintaining a residual load of above 60 kips.
2. The maximum factored live load condition, for heavy manufacturing or heavy storage warehouse applications per ASCE 7, equates to 20.8 kips (250psf multiplied by a load factor of 1.6 and the surface area of the concrete deck), therefore the specimens yielded at 4.3 to 5.1 times the maximum factored live load condition and failed at 4.6 to 5.3 times the maximum factored live load condition. Deflections at the maximum live load condition measured very small at less than $1/10^{th}$ of an inch, with L/480 slightly greater than $3/10^{th}$'s of an inch for the test spans; the deflections were well within the most stringent deflection code requirement for roof or floor construction supporting or attached to nonstructural elements likely to be damaged by large deflections

3. The strut and tie model was unable to accurately predict the shear compression failure of the specimens. The analytical flexural analysis of the system using measured strains shows less than 1% difference from the observed maximum moment of the system.
4. This thesis also presents a strut and tie model that predicts the behavior of the system while accounting for large voids in the concrete web. The loading of the model was incrementally increased until the geometric constraints of the specimen made it impossible for the struts and ties to transfer load. This occurred first at a load where compression strut transferring load across the top flange of the steel wide flange and tension tie transferring load across the bottom flange of the steel wide flange began to overlap. The model fails at 62% of the observed ultimate load of the system. The strut and tie model did not accurately predict the failure mode of the system in shear compression. The model fairly accurately predicts the load paths evidenced by concrete cracking in the specimens and shows that composite action of the steel and concrete sections cannot be maintained under the current layout and placement of mechanical openings.
5. It may be possible to improve shear capacity of the specimens through greater concrete confinement in the stem walls, and improved connections of reinforcement to the steel beam. For example, all of the specimens exhibited preliminary cracking around the nelson studs at the boundary of the end stem walls and the mechanical openings. The strut and tie model demonstrates the need for a significant tension tie in this region, placing vertical reinforcement at this

location that extends into the concrete deck would allow better transfer of tensile stresses at this location.

6. Changing the shape of the mechanical openings to one resembling a semi-circle or arc may create an arching effect that will both minimize the shear around the openings and create a tension tie at the base of the openings. The tension tie at the base of the arch would likely also improve the flexural capacity of the specimens and allow for improved composite performance.
7. Further testing of any modifications to the layout and reinforcement of the specimens should be undertaken to verify the improvements made.

APPENDIX

STRUT AND TIE MODEL CALCULATIONS

Web Calculations:

$V_u = 0.62 \cdot 50kip = 31\ kip$

$\alpha_1 = \text{atan}\left(\frac{29.75}{13.75}\right) = 65.194\ deg$ $\alpha_2 = \text{atan}\left(\frac{9.48}{11.667}\right) = 39.096\ deg$

$\alpha_3 = \text{atan}\left(\frac{20.27}{13.75}\right) = 55.849\ deg$ $\alpha_4 = \text{atan}\left(\frac{20.27}{12}\right) = 59.374\ deg$

$a = 6$ $b = 4$ $a + b = 1$

$AB = \frac{a \cdot V_u}{\sin(\alpha_1)} = 20.491\ kip\ comp$ $Aa = V_u \cdot b = 12.4\ kip\ comp$

$aB = \frac{Aa}{\sin(\alpha_3)} = 14.984\ kip\ comp$ $HI = \frac{V_u}{\sin(\alpha_4)} = 36.025\ kip\ comp$

$BC = aB \cdot \sin(\alpha_3) + AB \cdot \sin(\alpha_1) = 31\ kip\ tension$

$CD = \frac{BC}{\sin(\propto_2)} = 49.158\ kip\ comp$ $EF = CD$ $GH = CD$

$DE = CD \cdot \sin(\alpha_2) = 31\ kip\ tension$ $FG = DE$

Steel Bottom Chord Calculations:

$AC = AB \cdot \cos(\alpha_1) = 8.597\ kip\ tension$

$CE = CD \cdot \cos(\alpha_2) + AC = 46.748\ kip\ tension$

$EG = CE + EF \cdot \cos(\alpha_2) = 84.9\ kip\ tension$

$Gg = \text{EG} + GH \cdot \cos(\alpha_2) = 123.051\ kip\ tension$

Steel Top Chord Calculations$aD = aB \cdot \cos(\alpha_3) = 8.411\ kip\ tension$

$DF = CD \cdot \cos(\alpha_2) - \text{aD} = 29.74\ kip\ compression$

$FH = DF + EF \cdot \cos(\alpha_2) = 67.892\ kip\ compression$

$Hh = FH + GH \cdot \cos(\alpha_2) = 106.043\ kip\ compression$

Concrete Flange (Deck) Calculations:

$\theta_1 = \text{atan}\left(\frac{1}{2}\right) = 26.565\ \text{deg}$ $\theta_2 = \theta_1$

$B = aB \cdot \cos(\alpha_3) + AB \cdot \cos(\alpha_1) = 17.008\ kip\ joint\ force$

$BJ = \frac{B}{2\cos(\theta_1)} = 9.508\ kip\ compression$ $BK = BJ$

$JK = BJ \cdot \sin(\theta_1) = 4.252\ kip\ tension$

$I = HI \cdot \cos(\alpha_4) = 18.352 kip\ joint\ force$

$IM = \frac{I}{2 \cdot \cos(\theta_2)} = 10.259\ kip\ compression$ $IL = IM$

$LM = IM \cdot \sin(\theta_2) = 4.588\ kip\ tension$

Area Check/Width of Struts and Ties Calculations:

$f_2 = 0.75 \cdot 4950 = 3713 psi$ $f_y = 65\ ksi$ $t_{sweb} = 0.19\ in.$

$t_{deck} = 4\ in.$ $t_{web} = 4\ in.$

$w_{AB} = \frac{AB}{f_2 \cdot t_{web}} = 1.38\ in.$

$w_{SAB} = \frac{AB}{f_y \cdot t_{sweb}} = 1.659\ in.$

$w_{SAa} = \frac{Aa}{f_y \cdot t_{sweb}} = 1.004\ in.$

$$w_{aB} = \frac{aB}{f_2 \cdot t_{web}} = 1.009\ in.$$

$$w_{HI} = \frac{HI}{f_2 \cdot t_{web}} = 2.426\ in.$$

$As_{reqBC} = \frac{BC}{f_y} = 0.477\ in^2$ 3 - #4 bars provided i.e. 0.6 in^2

$$w_{SBC} = \frac{BC}{f_y \cdot t_{sweb}} = 2.51\ in.$$

$$w_{CD} = \frac{CD}{f_y \cdot t_{sweb}} = 3.98\ in.$$

$$w_{DE} = \frac{DE}{f_y \cdot t_{sweb}} = 2.51\ in.$$

Bottom Chord Area Requirements:

$$area_{AC} = \frac{AC}{f_y} = 0.132\ in^2$$

$$area_{CE} = \frac{CE}{f_y} = 0.719\ in^2$$

$$area_{EG} = \frac{EG}{f_y} = 1.306\ in^2$$

$$area_{Gg} = \frac{Gg}{f_y} = 1.893\ in^2$$

Top Chord Area Requirements:

$$area_{aD} = \frac{aD}{f_y} = 0.129\ in^2$$

$$area_{DF} = \frac{DF}{f_y} = 0.458\ in^2$$

$$area_{FH} = \frac{FH}{f_y} = 1.044\ in^2$$

$$area_{Hh} = \frac{Hh}{f_y} = 1.631\ in^2$$

$$area_{steel\_beam} = 3.54\ in^2$$

$$area_{Hh} + area_{Gg} 3.525\ in^2$$

Concrete Deck Width and Area Requirements:

$$w_{BJ} = \frac{BJ}{t_{deck} \cdot f_c'} = 0.48\ in.$$

$$As_{reqJK} = \frac{JK}{f_y} = 0.065\ in^2$$

$$w_{IL} = \frac{IL}{t_{deck} \cdot f_c'} = 0.518\ in.$$

$$As_{reqLM} = \frac{LM}{f_y} = 0.071\ in^2$$

REFERENCES

ACI Standard 318, 2002, Building code requirements for reinforced concrete (ACI 318-2002), American Concrete Institute, Detroit, MI

Tureyen, A. Koray, Frosch, Robert J., 2003, Concrete Shear Strength: Another Perspective, ACI Structural Journal, 100(5), 609-615.

Redwood, Richard, Demirdjian, Sevak, 1998, Castellated Beam Web Buckling in Shear, ASCE Journal of Structural Engineering, 124(10), 33-39.

Wight, James K., MacGregor, James G., 2008, Reinforced Concrete: Mechanics and Design 5th Edition, Prentice Hall, Pearsons Custom Library: Engineering Series.

Viest, Ivan M., Colaco, Joseph P., Furlong, Lawrence G. Griffs, Leon, Roberto T., Wyllie, Loring A., 1997, Composite Construction Design for Buildings, ASCE, New York, NY., McGraw-Hill.

Liang-Jenq, L., Chang-Wei, H., Chuin-Shan, C., & Ying-Po, L. (2006), Strut-and-Tie Design Methodology for Three-Dimensional Reinforced Concrete Structures. Journal of Structural Engineering, 132(6), 929-938.

ASCE Standard ASCE/SEI 7-05, 2005, Minimum design loads for buildings and other structures (ASCE 7-2005), American Society of Civil Engineers, USA

AISC Steel Construction Manual Thirteenth Edition, 2005, Steel Construction Manual (AISC 13), American Institute of Steel Construction, Inc., USA

Vecchio, Frank J., Collins, Michael P., 1986, The Modified Compression-Field Theory for Reinforced Concrete Elements Subjected to Shear, ACI Journal, March-April 1986, .219-231.